Journal of the American Ceramic Society / Volume 101, Issue 6

ORIGINAL ARTICLE | Open Access

Synthesis of group IV and V metal diboride nanocrystals via borothermal reduction with sodium borohydride

Luca Zoli, Pietro Galizia, Laura Silvestroni, Diletta Sciti

First published: 21 December 2017
https://doi.org/10.1111/jace.15401

Abstract

The synthesis of early transition nanocrystals using $NaBH_4$ and the respective metal oxides at atmospheric pressure was studied at temperatures between 400 and 1000°C. Reaction products were analyzed by x-ray diffraction, the crystallite size was determined after Rietveld refinement of diffraction patterns, while the morphology was analyzed by scanning and transmission electron microscopy. For all the investigated systems the lowest temperature to complete the synthesis was 700°C and the reaction occurred in three subsequent steps: (i) decomposition of $NaBH_4$, (ii) formation of crystalline ternary species Na–M–O and Na–B–O, (iii) conversion of intermediary species to MB_2 and $NaBO_2$. Syntheses carried out at T > 700°C only caused coarsening of the powders. The synthetized boride powders had the morphology of highly agglomerated nanocrystals. TiB_2 had a specific surface area of 33.5 m^2/g and crystallite diameter of 12 nm. Both ZrB_2 and HfB_2 had a platelet-like morphology with crystallite diameter around 45 nm and specific surface area of 25.0 and 36.4 m^2/g, respectively. Finally, NbB_2 and TaB_2 powders had a crystallite

1 INTRODUCTION

Group IV and V metal borides are ultra-refractory materials with melting temperatures above 3000°C, hard, thermally, and electrically conductive,[1] with high mechanical strength and rigidity up to 2000°C or higher[2] and are chemically stable in acidic environments.[3] Due to these excellent qualities, borides of early transition metals are considered candidates for aerospace applications, such as engine components and leading edges for hypersonic reentry vehicles. Other prospective uses include concentrated solar thermal absorbers,[4, 5] nuclear fuel cladding, and neutron absorbers.[6] In particular, combined with silicon carbide or carbon fiber as ceramic matrix composites (CMCs), they provide a combination of improved failure tolerance and ablation resistance.[7-9] Carbothermal reduction[10, 11] is a well-established synthesis used at the industrial scale, however, reactive processes or a chemical route are also promising approaches.[1, 12] Availability of submicrometric/nanometric boride particles offers the possibility to improve several stages of ceramic processing,[13] such as the sintering of bulk ceramics, due to enhanced particle reactivity,[14] or the infiltration of fiber preforms. Moreover, other properties of borides may benefit from a reduction in size, such as the catalytic behavior. Indeed the use of these borides as catalysts is a relatively unexplored field of research.[15] Recent studies report on the synthesis of group IV and V boride nanostructured powders by reactions of $NaBH_4$ with $TiCl_4$, $ZrCl_4$, $HfCl_4$, and $NbCl_5$ at 600-700°C under autogenic pressure,[16-19] while Portehault and co-worker introduced the reaction of $NbCl_5$, $HfCl_4$, $CaCl_2$, $CeCl_3$, $MoCl_5$, $FeCl_2$, $MnCl_2$, and $NaBH_4$ under atmospheric pressure using LiCl/KCl molten salt at 900°C for 4 hours.[20] Synthesis of metal diborides via reduction in metal oxides using polyborane was proposed by Forsthoefel and Sneddon [21] to produce group IV and V MB_2 crystals with size <1.0 μm. Few groups focused their activity on NbB_2: Jha et al[22] used NbO_2 with elemental boron via solid-state reaction to obtain nanorods (40 × 800 nm^2), Ran and co-worker combined Nb_2O_5, B and NaCl/KCl to produce nanocrystals (61 nm).[23] Ma et al[24] obtained nanocrystals of NbB_2 via thermal reduction in Nb_2O_5, H_3BO_3, at 650°C for 10 hours using NaCl/$MgCl_2$ as molten salt. Finally a carbo-thermal reduction was proposed by Maeda et al[25] by the use of Cornstarch as carbon source to obtain nanometric NbB_2 at 1700°C. Interestingly Chen ad co-workers [26] achieved TiB_2 and ZrB_2 crystals with size of 100 nm and 500 nm, respectively, and micrometric NbB_2 (5 μm) via a boro-thermal reduction in the corresponding metal oxides with elemental boron assisted by Na and S. Despite the large variety of syntheses proposed, to the best of the authors' knowledge, the use of metal

with $NaBH_4$ under vacuum at 1200°C, while by Pan et al[29] using lanthanum hydroxide or oxide with $LiBH_4$. De Resende et al[30] produced Fe-B alloys combining nano-sized goethite (α-FeOOH) in acid solution with $NaBH_4$. Finally, CrB was obtained by Wao and co-worker sealing Cr_2O_3 and $NaBH_4$ in autoclave for 10 hours at 600°C.[31]

In our previous work, for the first time, we produced ZrB_2 nanocrystals at 900°C, starting from a mixture of ZrO_2 and $NaBH_4$.[32] Here, we extend the use of $NaBH_4$ to group IV and V metal oxides to demonstrate the general validity of this synthesis even in a lower temperature range, for example, 500-700°C. The main goal of this method is the use of cheap raw materials and mild conditions to achieve nano-borides.

2 EXPERIMENTAL PROCEDURE

Commercial $NaBH_4$ (Fluka, purity ≥ 98%, Silica ≤ 100 ppm, Fe ≤ 55 ppm), TiO_2 (Degussa P25, Ca ≤ 0.1%, K ≤ 100 ppm, Fe, Cr ≤ 300 ppm), ZrO_2 (Carlo Erba, purity >99.99%), HfO_2 (Johnson), Nb_2O_5 (Sigma Aldrich, ≤ 45 μm, purity >99,9%, metallic impurities ≤1500 ppm) and Ta_2O_5 (Sigma Aldrich, ≤ 20 μm, 99.99%, metallic impurities ≤150 ppm) were used for the synthesis. The raw metal oxides were characterized as follows. The particle size distribution (D_{50}) was measured using the sedimentation method (SEDIGRAPH III 5125 plus, USA), the specific surface area (s.s.a.) by the BET method (Surfer apparatus, Thermo Scientific), the morphology was analyzed by Field Emission Scanning Electron Microscopy (FE-SEM Carl Zeiss Sigma NTS Gmbh Öberkochen, Germany) equipped with energy dispersive spectroscopy (EDS, INCA Energy 300, Oxford Instruments, UK).

For the syntheses the following procedure was adopted. Before heating, 10.00 g of sodium borohydride was finely ground in a mortar and then gently mixed with the metal oxide (M: B molar ratio 1:4) in polyethylene bottles with zirconia milling media (balls: powders 10:1 mass ratio) with diameter of 5 mm for 4 hours at 60 rpm and placed in a zirconia crucible. All the syntheses were carried out in alumina tubular furnace (Nabertherm, Germany) under argon atmosphere, with heating rate of 3 °C/min up to the target temperature, holding time of 30 minutes and free cooling. In the case of ZrB_2 the synthesis was carried out at 400, 500, 600, 700, 800, 900, and 1000°C. On the basis of the results obtained with ZrO_2-$NaBH_4$ system, experiments with TiO_2, HfO_2, Nb_2O_5, and Ta_2O_5 were only conducted at the temperatures of interest, namely, 500 and 700°C. X-Ray diffraction (XRD) patterns of as-synthesized powders were collected by a Bruker D8 Advance X-ray diffractometer (θ-θ) equipped with a LINXEYE

aim, the powders synthesized at 700°C were washed with hot water three times to remove unwanted Na-based phases from boride nanocrystals products and dried under vacuum at 100°C for 12 hours. The ZrB_2 washed synthesized at 700°C powders were dissolved in hot nitric acid and the residual unwanted Na-based phases were determined by Inductively Coupled Plasma Optical Emission Spectrometry (ICP-OES) and expressed as ppm of Na. The peak profiles were fitted using pseudo-Voigt with Finger - Cox - Jephcoat peak asymmetry function (GSAS profile: type 3) while a sixth-order polynomial equation was used to fit the background. In order to quantify the length of the crystallites, along the orthogonal directions, <100 > and <001 > we applied the Scherrer's formula on the (100) and (001) peaks, respectively: 34 $D = \lambda/(\beta \cos\theta)$, where λ is the Cu Kα wavelength, β is the Lorentzian broadening contribution on the integral breadth of the XRD peaks and *D* is the volume-weighted crystallite size perpendicular to the diffraction plane, with the Scherrer's constant fixed to one. The structures of crystal lattice and crystallite shape were sketched by VESTA software.35 Specific surface area (*s.s.a.)* of the reaction products at 700°C was measured by the BET method. The morphologies of as-synthesized powders were analyzed by SEM-EDS. In addition, ZrB_2 powders synthesized at 700°C were observed in transmission electron microscopy (TEM, JEOL JEM 2100F, Tokyo, Japan) operating at a nominal voltage of 200 kV and equipped with an energy-dispersive X-ray system (EDS, mod. INCA Energy 300, Oxford instruments, UK). The powders were deposited on holey carbon film coated copper grid through a vacuum apparatus and immediately observed using a transmission electron microscope. Electron diffraction patterns identification was carried out through the software tool developed for Digital Micrograph.36

3 RESULTS AND DISCUSSION

Characterization of starting metal oxides was reported in Table S1, oxides powders had a D_{50} in the submicrometric range. SEM images, see Figure S1, show that the particles are highly agglomerated, especially in the case of TiO_2.

As previously mentioned, we extensively studied the ZrO_2-$NaBH_4$ system, and then extended the synthesis to other borides, with the aim of drawing common steps.

ZrO_2-based system. XRD patterns for the powders synthesized from 400 to 1000°C are shown in Figure 1.

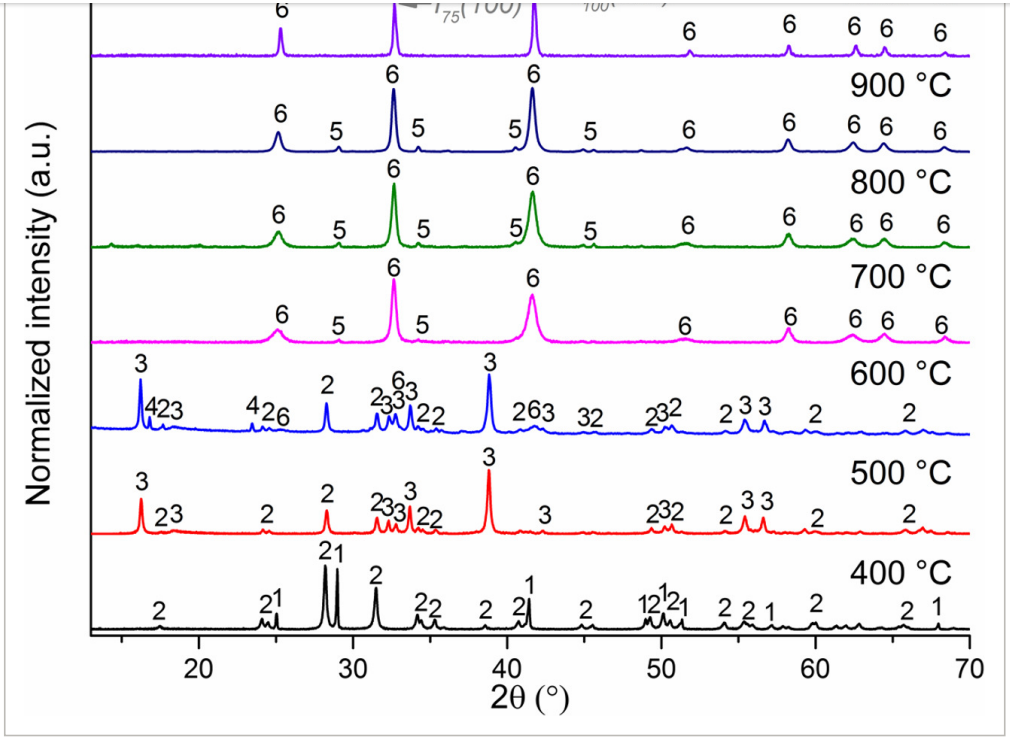

Figure 1

Open in figure viewer | PowerPoint

XRD patterns of ZrO_2-$NaBH_4$ system after synthesis for 30 min at 400-1000°C. Arrows evidence the change in relative peaks intensity (100 and 75%) of the ZrB_2 phase passing from 700 to 1000°C synthesis temperature [Color figure can be viewed at wileyonlinelibrary.com]

Caption

After synthesis at 400°C reflections of the starting species, monoclinic ZrO_2 and cubic $NaBH_4$, were still well detectable, indicating that no reaction had occurred yet. On the contrary, after synthesis at 500°C we observed the lack of $NaBH_4$ reflections and the formation of a new Na-Zr-O intermediate specie, labeled as monoclinic sodium zirconate (Na_2ZrO_3, ICCD: 35-0770).[37] With increasing the synthesis temperature to 600°C, ZrO_2 and Na_2ZrO_3 were still detected, however, it was already possible to recognize broad reflections associated to the crystals

appearance of rhombohedral sodium meta-borate ($NaBO_2$, ICCD: 32-1046), as side-product. From this key temperature on, no further phase transformations of boride products was observed.

After synthesis at T > 1000°C, $NaBO_2$ diffraction peaks were no longer observed, owing to melting and partial evaporation.[38] However, residual traces of this phase below the XRD resolution limit (~3%-4%) cannot be ruled out. In addition, XRD analyses gave some preliminary indications about the morphology of the new-born crystals, subsequently confirmed by microscopic analysis. The peaks intensity associated to (100) and (101) crystal plans of ZrB_2 perfectly matched the theoretical ones only after 1000°C synthesis. Instead, at lower temperatures (700-900°C) the main reflection, I_{100} (101), had a lower intensity than I_{75} (100), (Figure 1). This could be associated with a distortion of the unit cell at early stages of the synthesis or could be due to Na cation inclusions. To understand the sodium contamination in the synthesized diboride we performed ICP-OES after synthesis at 700°C. The analyses confirmed that the Na content was <10 ppm after 3° washing procedure.

TiO_2, HfO_2, Nb_2O_5, and Ta_2O_5 based systems. XRD patterns of the powders after synthesis at 500 and 700°C are reported in Figure 2.

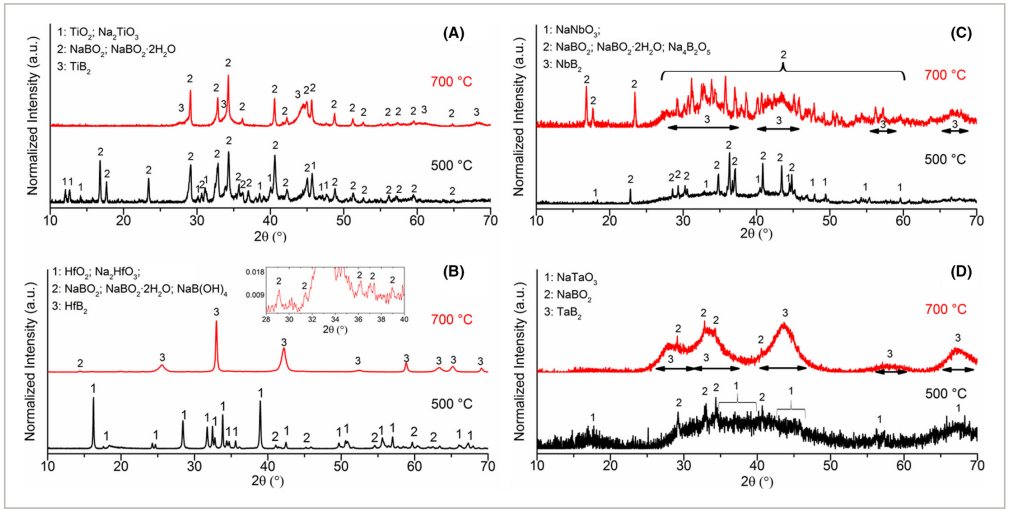

Figure 2

due to the air exposure during the X-ray analysis [Color figure can be viewed at wileyonlinelibrary.com]

Caption

Patterns collected after synthesis at 500°C show the formation of two types of ternary phases with general formula $Na_xM_yO_z$ and $Na_xB_yO_z$. After synthesis at 700°C the complete conversion of starting metal oxides and intermediate products to metal boride nanocrystals occurred in analogy with the ZrO_2-system. In detail:

1. Monoclinic titanium oxide (TiO_2, ICDD 48-1278), sodium titanate (Na_2TiO_3, ICDD 37-0346) and sodium borate hydrate ($NaBO_2{\cdot}2H_2O$, ICDD: 06-0122), were detected at 500°C; hexagonal titanium boride (TiB_2, ICDD: 35-0741) and sodium meta-borate ($NaBO_2$, ICDD: 32-1046), were detected at 700°C in the TiO_2 system, Figure 2A;
2. monoclinic hafnium oxide (HfO_2, ICDD: 34-0104), sodium hafnate (Na_2HfO_3, ICDD: 016–0597) and sodium borate hydrate ($NaBO_2{\cdot}2H_2O$, ICDD: 06-0122) were recorded at 500°C; sodium meta-borate ($NaBO_2$, ICDD: 32-1046), sodium tetrahydroxyborate ($NaB(OH)_4$, ICDD: 81-1512), and hexagonal hafnium boride (HfB_2, ICDD: 38-1398) were visible at 700°C in the HfO_2 system, Figure 2B;
3. Reflections of monoclinic sodium borate ($Na_2B_4O_5$, ICDD: 36-0878) and natroniobite ($NaNbO_3$, ICDD: 26-1380) were visible at 500°C while hexagonal niobium boride (NbB_2, ICDD: 35-0742), sodium meta-borate ($NaBO_2$, ICDD: 32-1046) and sodium borate hydrate ($NaBO_2{\cdot}2H_2O$, ICDD: 06-0122) were detected at 700°C in the Nb_2O_5 system, Figure 2C.
4. Broad reflections of sodium tantalum oxide ($NaTaO_3$, ICDD: 25-0863) and hexagonal tantalum boride (NbB_2, ICDD: 38-1462) were recognized at 500°C and at 700°C, respectively, while sodium meta-borate ($NaBO_2$, ICDD: 32-1046) was revealed at both temperatures in the Ta_2O_5 system, Figure 2D.

Refined XRD patterns of the washed powders obtained at 700°C, for all the investigated systems are reported in Figure 3. Table 1 reports lattice constants average crystallite sizes, ($D_{(100)}$) and ($D_{(001)}$), along the *c* and *a* axes, respectively, crystallographic density and other relevant parameters obtained through the Rietveld refinement. The as-refined parameters, shown in Table 1, take into account the shape of the crystallites as the aspect ratio strongly affects the diffraction peaks.

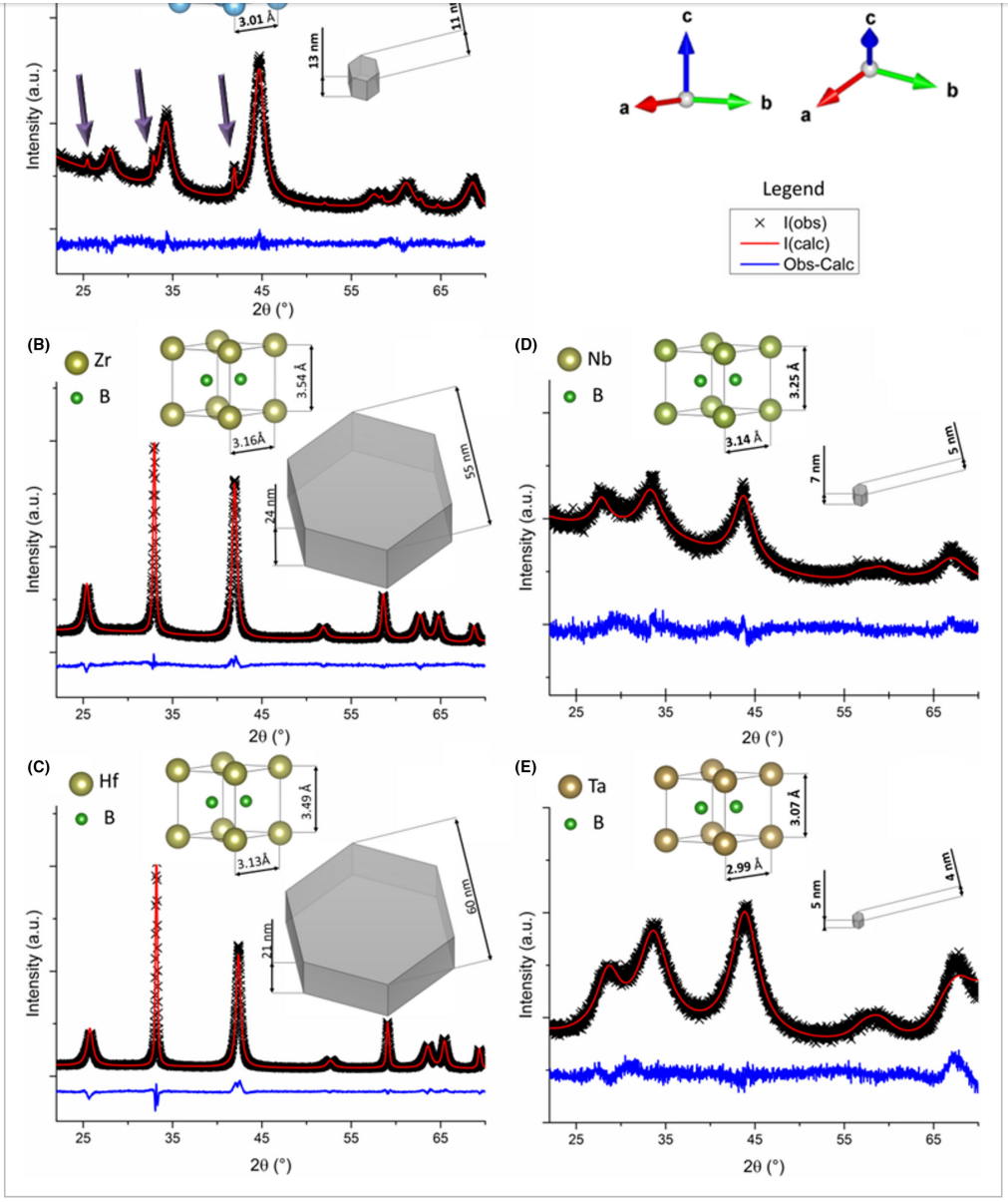

Figure 3

Open in figure viewer | PowerPoint

NbB_2 (c) TaB_2. Arrows highlights spurious ZrB_2 peaks in HfB_2 powder due to ZrO_2 contamination

[Color figure can be viewed at wileyonlinelibrary.com]

Caption

Table 1. Characteristics of produced metal borides: lattice parameter (*a*), axial ratio (*c/a*), crystallographic density (ρ_x), average crystallite sizes, ($D_{(1\,0\,0)}$) and ($D_{(0\,0\,1)}$) along <1 0 0 > and <0 0 1 > directions, aspect ratio ($R = D_{(1\,0\,0)}/D_{(0\,0\,1)}$), anisotropic broadening rectification (GSAS profile term: *ptec*), equivalent sphere diameter of the crystallite (D). χ^2 is the fit goodness and depicts the refinement fitting parameters, specific surface area (BET)

	a Å	*c/a*	ρ_x (g/cm^3)	$D_{(1\,0\,0)}$ (nm)	$D_{(0\,0\,1)}$ (nm)	*R*	*ptec*	*D* (nm)	χ^2	*s.s.a.* (m^2/g)
TiB_2	3.01	1.06	4.61	11	13	0.8	−22.91	12	1.23	33.45
ZrB_2	3.16	1.12	6.12	55	24	2.3	41.71	45	3.14	24.97
HfB_2	3.13	1.11	11.20	60	21	2.9	56.74	45	4.15	36.36
NbB_2	3.14	1.04	6.84	5	7	0.7	−85.33	6	1.49	21.09
TaB_2	2.99	1.03	14.13	4	5	0.8	−79.93	5	1.18	11.38

The equivalent spherical diameter, *D*, and the aspect ratio, $R = D_{(100)} / D_{(001)}$, quantify size and morphology of the crystallites which range between 5 and 45 nm and result plate-like ($R > 1$) or columnar-like ($0 < R < 1$). In agreement with the microscopy analysis, TiB_2, NbB_2, and TaB_2 show a columnar-like shape, while ZrB_2 and HfB_2 present a plate-like shape.

3.1 Microstructural characterization

Morphological analysis of the ZrO_2-$NaBH_4$ system synthesized at 400, 500, 600, and 700°C is reported in Figure 4, morphologies of the other metal oxides-$NaBH_4$ systems synthesized at 700°C are shown in Figure 5. Specific surface area values for synthesis at 700°C are summarized in Table 1 and range from 11 to 34 m^2/g. Worthy to mention, the synthesized

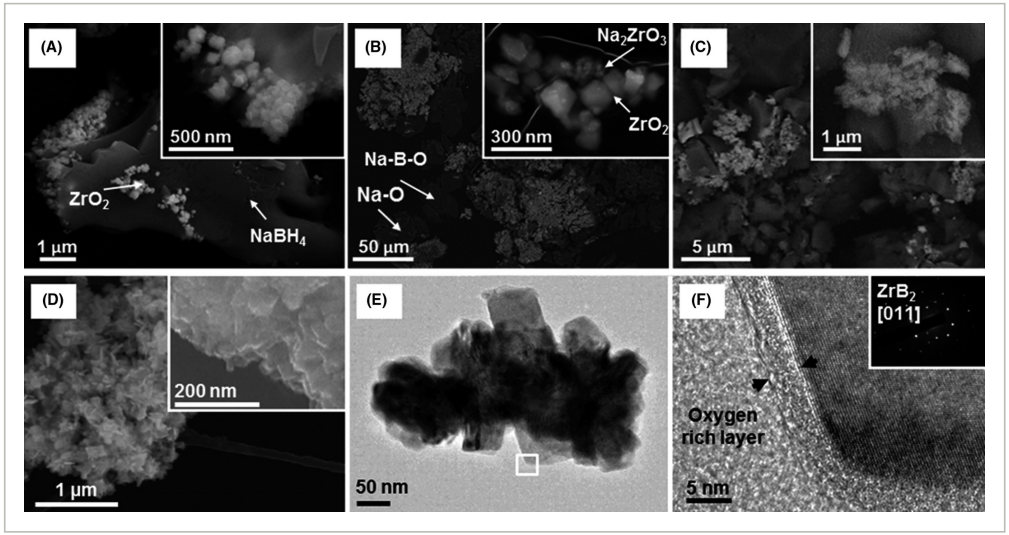

Figure 4

Open in figure viewer | PowerPoint

SEM image of the ZrO_2-$NaBH_4$ system after synthesis at (A) 400°C, (B) 500°C, (C) 600°C, (D) 700°C. For this last powder, (E) the corresponding bright field TEM, (F) high-resolution image and diffraction pattern (inset in F) are provided. Arrows in the HR-TEM image in (F) points to oxygen-rich layer around ZrB_2 platelet

Caption

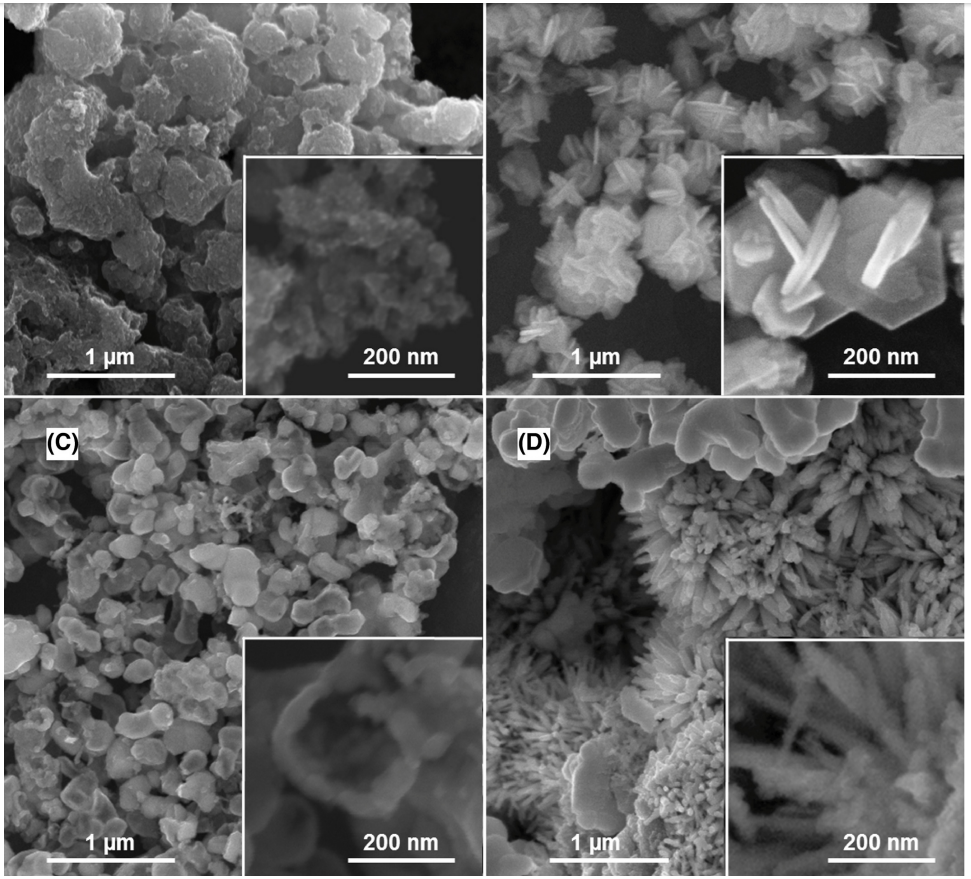

Figure 5

Open in figure viewer | PowerPoint

SEM images of powders after synthesis at 700°C for (A) TiO_2-$NaBH_4$, (B) HfO_2-$NaBH_4$, (C) Nb_2O_5-$NaBH_4$, (D) Ta_2O_5-$NaBH_4$. The insets are magnified images of the corresponding powder

Caption

3.1.1 ZrB_2

For the ZrO_2-based system we tried to follow all the stages of the synthesis up to 1000°C. The morphology of powders after synthesis at 400°C is shown in Figure 4A: submicrometric

images by SEM. Amorphous Na–B–O and Na–O (with dark contrast) are well distinguishable from crystalline ZrO_2 and Na_2ZrO_3 phases (bright contrast). From microstructural investigation we deduced that Na_2ZrO_3 intermediate specie nucleated on the edges of ZrO_2 particles, inset Figure 4B. At 600°C the fuzziness aspect of ZrO_2 or Na_2ZrO_3 nanocrystals further increased, as perceivable from the inset of Figure 4C. Morphology analysis of the as-synthesized powder at 700°C, SEM analysis in Figure 4D, shows a micron-sized agglomerate constituted of randomly oriented nano-platelets. In Figure 4E, TEM analysis of a polycrystalline sub-micrometer particle shows nano-platelets crystals with faceted shape around 50 nm and each ZrB_2 crystal was continuously surrounded by an amorphous oxygen-rich layer, as shown in the HR-TEM image of Figure 4F. This powder has a specific surface area of 25 m^2/g, Table 1. After synthesis at temperature >700°C we just observed an increase in the boride crystal size. At 1000°C (not shown) we observed ordered platelets, ~200 nm wide and ~20 nm thick.

3.1.2 TiB_2

The powder obtained at 700°C (Figure 5A) consisted of rounded micron-sized particles highly agglomerated, the nanostructure of a TiB_2 cluster shown in the inset of Figure 5A has an average crystal size around 20 nm. This powder has a specific surface area of 33 m^2/g, (Table 1) similar to that reported by Shi, 25.93 m^2/g.[39]

3.1.3 HfB_2

The product obtained at 700°C (Figure 5B) consists of polycrystalline particles having size of 1-2 μm, with rose-like morphology. Nano-platelets have size below 200 nm and thickness of tens of nm (inset of Figure 5B). The specific surface area is 36 m^2/g. As far as we know, this particular rose-like morphology has never been reported before for HfB_2,[18,20] and could be a suitable morphology for application as catalysts.

3.1.4 NbB_2

The micrograph in Figure 5C shows micron-sized particles constituted of rounded hollow clusters weakly bonded having size around 200 nm. Inset of Figure 5C highlighted the core of an hollow nanostructured aggregates with crystallite size of few nm according to XRD analysis. The powder has a specific surface area of 21.08 m^2/g. Portehault et al[20] obtained NbB_2 powders with size and *s.s.a*. analogue to our results by heat treatment of $NbCl_5$ and $NaBH_4$ in molten salt (LiCl/KCl) at atmospheric pressure and 900°C for 4 hours (e.g., 10 nm, 25 m^2/g, M:B = 1:4). Ran and co-worker [23] used Nb_2O_5 and amorphous B in molten salts (NaCl/KCl) to

3.1.5 TaB_2

SEM analysis revealed two different morphology of particles, needles and rounded poly-crystalline particles (Figure 5D), which may be due to local variation in chemistry and pressure conditions. Rounded particles have a size around 300 nm, needles have a max length of around 200 nm and thickness of few nm. The nanostructure of needles particles is highlighted in inset of Figure 5D, according to XRD analysis the crystallite size is below 20 nm, similar observation are valid for rounded particles. This powder has a specific surface area of 11.38 m^2/g, which to the best of our knowledge it is the highest value reported in literature.[13, 40]

3.2 Thermodynamic calculation

To get a general overview on the reaction path for the synthesis of transition metal borides, thermodynamic calculations were performed through the commercial package HSC Chemistry v. 6.1 (Outokumpu Research Oy, Pori, Finland).

According to information collected from XRD and the thermodynamic computations, the overall reactions describing the synthesis can be written as follows, depending if we deal with tetravalent metal oxides (Zr, Ti, Hf), reaction 1, or pentavalent metal oxides (Ta, Nb), reaction 2:

$$MO_2 + 3NaBH_4 = MB_2 + 2Na(l,g) + NaBO_2 + 6H_2(g) \quad (1)$$

$$M_2O_5 + 6.5NaBH_4 = \ 2MB_2 + 4Na(l,g) + 2.5NaBO_2 + 13H_2(g) \quad (2)$$

where the gaseous product, H_2 and Na above 900°C volatilize and the solid byproducts, $NaBO_2$, can be washed away by hot water. If we plot the free Gibbs energy, ΔG, of reactions 1 and 2 for all the systems considered as a function of the temperature, Figure 6, we observe that for pentavalent metals the reactions is favorable at any temperature, for Ti it becomes favorable at 150°C, while for Zr and Hf above 300°C. Therefore, from a mere thermodynamic point of view, the conversion from oxide to boride it is favored at extremely low temperatures.

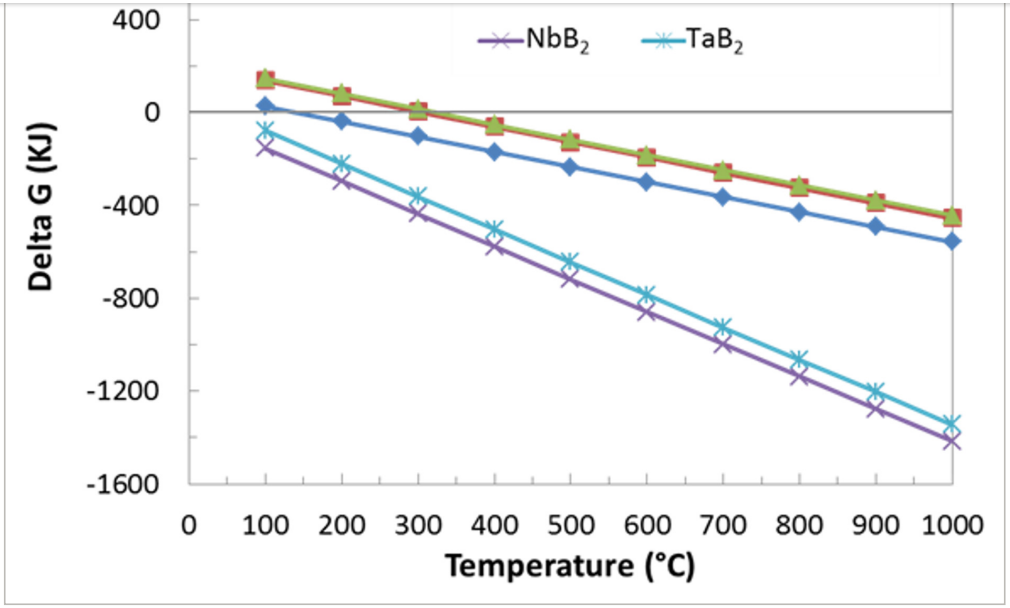

Figure 6

Open in figure viewer | PowerPoint

Gibbs free energy of reactions 1 and 2 as a function of temperature and type of metal oxide

[Color figure can be viewed at wileyonlinelibrary.com]

Caption

HSC Chemistry v.6.1 was used also to plot the isobaric multiphase equilibria vs temperature diagrams of the systems investigated except for HfO_2 because Na_2HfO_3 is not available in its database. A batch of possible species were selected for the computation (e.g., B_2O_3, Na_2O, B, $NaBO_2$, $NaMO_3$, Na_2MO_3 etc.), the initial conditions set are atmospheric pressure plus 0.1 mol. argon and H_2 and the amount of the reagents defined by reaction 1 for ZrO_2- and TiO_2-systems and by reaction 2 for Nb_2O_5- and Ta_2O_5-systems, see Figure 7.

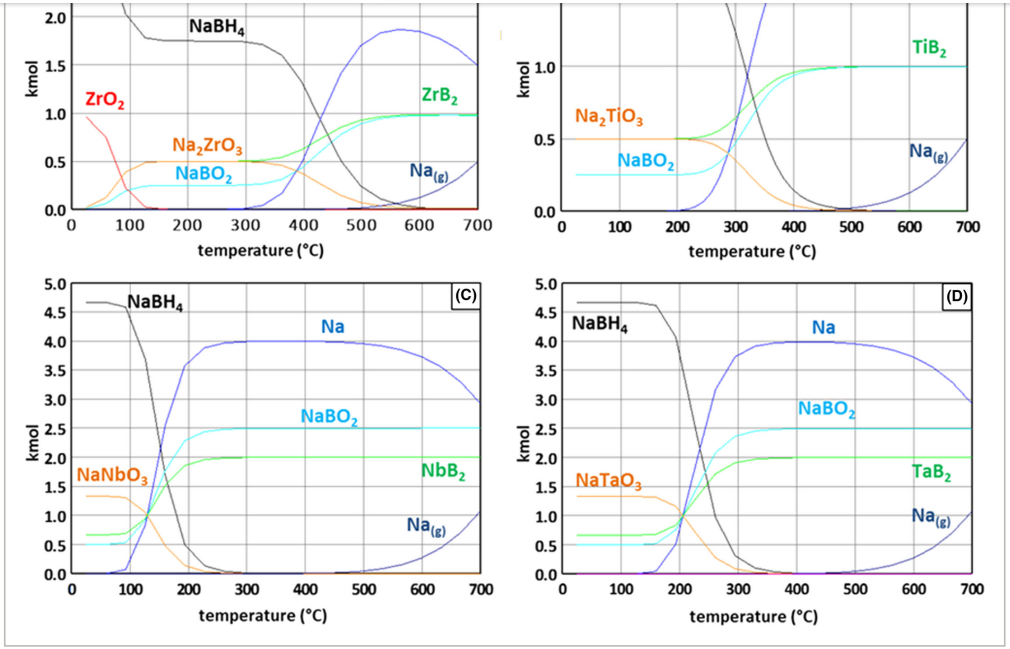

Figure 7

Open in figure viewer | PowerPoint

Isobaric multiphase equilibria as function of the temperature calculated using HSC Chemistry v.6.1 for the systems investigated and available in the database: (A) ZrO_2-$NaBH_4$, (B) TiO_2-$NaBH_4$, (C) Nb_2O_5-$NaBH_4$, (D) Ta_2O_5-$NaBH_4$ [Color figure can be viewed at wileyonlinelibrary.com]

Caption

Although decomposition of $NaBH_4$ and formation of Na-M-O species are forecast at a premature range of temperature compared to XRD data, the phase equilibria reported in Figure 7 well agree with the crystalline phases observed in the temperature range 400-700°C. Formation of Na–M–O and Na–B–O can be explained by the sequence of reactions (3)-(7) reported in Table 2, that also discriminates MO_2 and M_2O_5-based systems. First, $NaBH_4$ decompose into Na, B, and gaseous hydrogen close to 500°C,41 reaction (3) in Table 2, and at this temperature, boron readily reacts with the solid metal oxides yielding boron oxide and metal diboride, reactions (4) in Table 2. Boron oxide so formed reacts with the available Na

Table 2. Sequence of reaction explain the formation of intermediate and final products

MO_2	M_2O_5	Reaction
$NaBH_4 = Na(l) + B(s) + 2H_2(g)$		3
$3MO_2 + 10B = 3MB_2 + 2B_2O_3$	$3M_2O_5 + 22B = 6MB_2 + 5B_2O_3$	4
$6Na + B_2O_3 = 3Na_2O + 2B$		5
$Na_2O + MO_2 = Na_2MO_3$	$Na_2O + M_2O_5 = 2NaMO_3$	6
$Na_2O + B_2O_3 = 2NaBO_2$		7

Actually we did not observed Na_2O as a crystalline product in XRD patterns, but we detected Na–O species by EDS (see Figure 4B), which suggests that this species could be involved in the reaction path as amorphous. Finally, it has to be remarked that in the present case, the proposed reaction path, through formation of the Na_2MO_3 phase for Ti, Zr; Hf and $NaMO_3$ for Nb and Ta, enables a remarkable decrease in synthesis temperature, only 700°C, for the obtainment of MB_2. Usually, metal oxides thermally treated with elemental boron powder provide the corresponding boride at temperature ≥1000°C, see ZrO_2 42 and Nb_2O_5.23 Therefore, it is plausible to suppose that the Na–M–O phases play a key role in these syntheses. Further studies with in situ X-ray diffraction focused on the effective role of intermediate products at relevant temperatures will be object of future works.

4 CONCLUSIONS

For the first time, we investigated the chemistry of $NaBH_4$ with a variety of IV and V group transition metal oxides to obtain the corresponding diboride nano-crystalline powders, TiB_2, ZrB_2, HfB_2, NbB_2 and TaB_2 at 700°C and atmospheric pressure. For all the systems under analysis, we identified the common reaction path which relies in the formation of intermediary Na–M–O species. Remarkably, irrespective of the different oxide starting phases, all the synthesized powders have a nanometric size of the crystallite ranging from 5 to 45 nm. The post synthesis Na-contamination can be efficiently removed with repeated washing cycles in

The choice of synthesis method requires balancing factors that include cost, purity, and crystallite size with respect to the performance needed in applications. In this regard, the use of the mild synthesis conditions here presented that enables easy adjustments of the crystallite size and shape is an excellent combination never achieved heretofore with previous routes. The atmospheric pressure and the use of cheap raw materials, like metal oxides and $NaBH_4$, are key points in order to move this method toward industrial scale-up.

ACKNOWLEDGMENTS

The research leading to these results has received funding from the European Union's Horizon 2020 Programme under grant agreement C3HARME No. 685594. The authors are grateful to A. Piancastelli and P. Pinasco, M. Mazzocchi for technical support.

SUPPORT INFORMATION

Supplementary File
Synthesis of Group IV and V Metal Diboride Nanocrystals via Borothermal reduction with sodium borohydride

Luca Zoli, Pietro Galizia, Laura Silvestroni and Diletta Sciti
Institute of Science and Technology for Ceramics (ISTEC), National Research Council (CNR), Via Granarolo 64, 48018, Faenza, Italy.

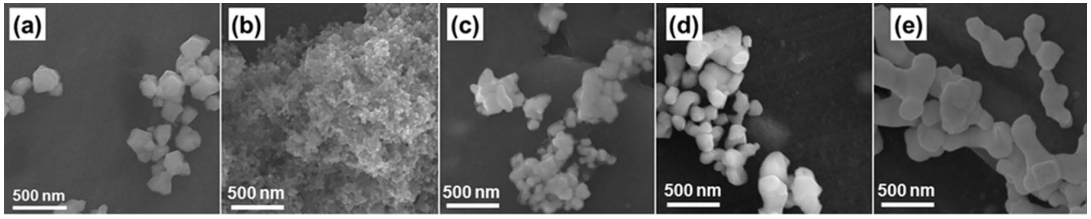

Figure S1 - SEM pictures of metal oxide used as raw materials: (a) ZrO_2, (b) TiO_2, (c) HfO_2 , (d) Nb_2O_5, (e) Ta_2O_5 powders.

Table S1 – Characteristics of the starting oxides. D50: particles size distribution (Sedigraph), m.g.s.: mean grain size (by SEM), s.s.a.: specific surface area (BET).

	D_{50} (µm)	m.g.s. (nm)	s.s.a. (m^2/g)
TiO_2	0.25	30	48.41
ZrO_2	0.56	110	9.46
HfO_2	0.51	150	4.18
Nb_2O_5	0.47	180	7.26
Ta_2O_5	0.79	300	2.44

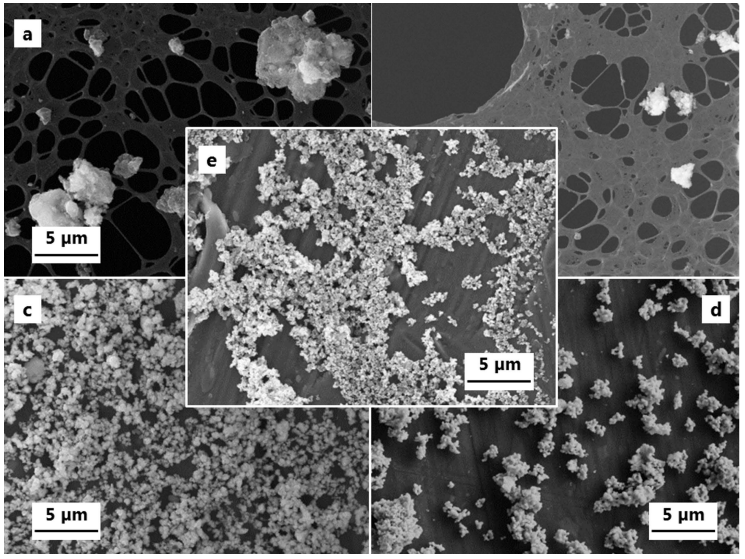

Figure S2- SEM pictures at low magnification of washed powders after wynthesis at 700 °C: (a) ZrB_2, (b) TiB_2, (c) HfB_2 , (d) NbB_2, (e) TaB_2.

REFERENCES

1 Fahrenholtz WG, Hilmas GE, Talmy IG, et al. Refractory diborides of zirconium and hafnium. *J Am Ceram Soc*. 2007;**90**:1347-1364.
Wiley Online Library | CAS | Web of Science® | Google Scholar

composite in aqueous solutions. *Electrochim Acta*. 2005;**50**:461-3469.
Crossref | Web of Science® | Google Scholar

4 Sciti D, Silvestroni L, Mercatelli L, et al. Suitability of ultra-refractory diboride ceramics as absorbers for solar energy applications. *Sol Energ Mat Sol C*. 2013;**109**:8-16.
Crossref | CAS | Web of Science® | Google Scholar

5 Pierrat B, Balat-Pichelin M, Silvestroni L, et al. High temperature oxidation of ZrC-20%$MoSi_2$ in air for future solar receivers. *Sol Energ Mat Sol C*. 2011;**95**:2228-2237.
Crossref | CAS | Web of Science® | Google Scholar

6 Lee WE, Gilbert M, Murphy ST, et al. Opportunities for advanced ceramics and composites in the nuclear sector. *J Am Ceram Soc*. 2013;**96**:2005-2030.
Wiley Online Library | CAS | Web of Science® | Google Scholar

7 Zoli L, Medri V, Sciti D, et al. Continuous SiC fibers-ZrB_2 composites. *J Eur Ceram Soc*. 2015;**35**:4371-4376.
Crossref | CAS | Web of Science® | Google Scholar

8 Sciti D, Zoli L, Silvestroni L, et al. Design, fabrication and high velocity oxy-fuel torch tests of a Cf-ZrB_2- fiber nozzle to evaluate its potential in rocket motors. *Mat Design*. 2016;**109**:709-717.
Crossref | CAS | Web of Science® | Google Scholar

9 Zoli L, Sciti D. Efficacy of a ZrB_2–SiC matrix in protecting C fibres from oxidation in novel UHTCMC materials. *Mat Design*. 2017;**113**:207-213.
Crossref | CAS | Web of Science® | Google Scholar

10 Jung EY, Kim JH, Jung SH, et al. Synthesis of ZrB_2 powders by carbothermal and borothermal reduction. *J Alloy Compd*. 2012;**538**:164-168
Crossref | CAS | Web of Science® | Google Scholar

11 Zhu XQ, Hu J, Zhang WJ, et al. Preparation and characterization of ultra-fine ZrB_2 powders from inorganic-organic hybrid precursors via carbothermal reduction. *Key Eng Mater*. 2016;**697**:54-57.
Crossref | Google Scholar

developments and perspectives. *Chem Rev*. 2013;**113**:7981-8065.
Crossref | CAS | PubMed | Web of Science® | Google Scholar

14 Sonber JK, Suri AK. Synthesis and consolidation of zirconium diboride: review. *Adv Appl Ceram*. 2011;**110**:321-334.
Crossref | CAS | Web of Science® | Google Scholar

15 Wu P, Lv H, Peng T, et al. Nano conductive ceramic wedged graphene composites as highly efficient metal supports for oxygen reduction. *Sci Rep*. 2014;**4**:3968.
Crossref | PubMed | Web of Science® | Google Scholar

16 Chen L, Gu Y, Qian Y, et al. A facile one-step route to nanocrystalline TiB_2 powders. *Mater Res Bull*. 2004;**39**:609-613.
Crossref | CAS | PubMed | Web of Science® | Google Scholar

17 Chen L, Gu Y, Yang Z, et al. Preparation and some properties of nanocrystalline ZrB_2 powders. *Scripta Mater*. 2004;**50**:959-961.
Crossref | CAS | Web of Science® | Google Scholar

18 Chen L, Gu Y, Shi L, et al. Synthesis and oxidation of nanocrystalline HfB_2. *J Alloy Compd*. 2004;**368**:353-356.
Crossref | CAS | Web of Science® | Google Scholar

19 Cai P, Yang Z, Shi L, et al. Low temperature synthesis of NbB_2 nanorods by a solid-state reaction route. *Mater Lett*. 2005;**59**:3550-3552.
Crossref | CAS | Web of Science® | Google Scholar

20 Portehault D, Devi S, Beaunier P, et al. A general solution route toward metal boride nanocrystals. *Angew Chem Int Edit*. 2011;**50**:3262-3265.
Wiley Online Library | CAS | PubMed | Web of Science® | Google Scholar

21 Forsthoefel K, Sneddon LG. Precursor routes to Group 4 metal borides, and metal boride/carbide and metal boride/nitride composites. *J Mater Sci*. 2004;**39**:6043-6049.
Crossref | CAS | Web of Science® | Google Scholar

borothermal reduction in molten salt. *J Am Ceram Soc*. 2014;**97**:3384-3387.
Wiley Online Library | CAS | Web of Science® | Google Scholar

24 Ma J, Du Y, Wu M, et al. A simple inorganic-solvent-thermal route to nanocrystalline niobium diboride. *J Alloy Compd*. 2009;**468**:473-476.
Crossref | CAS | Web of Science® | Google Scholar

25 Maeda H, Yoshikawa T, Kusakabe K, et al. Synthesis of ultrafine NbB_2 powder by rapid carbothermal reduction in a vertical tubular reactor. *J Alloy Compd*. 1994;**215**:127-134.
Crossref | CAS | Web of Science® | Google Scholar

26 Chen B, Yang L, Heng H, et al. Additive-assisted synthesis of boride, carbide, and nitride micro/nanocrystals. *J Solid State Chem*. 2012;**194**:219-224.
Crossref | CAS | Web of Science® | Google Scholar

27 Li Y, Fan Y, Chen Y. A novel route to nanosized molybdenum boride and carbide and/or metallic molybdenum by thermo-synthesis method from MoO_3, KBH_4, and CCl_4. *J Solid State Chem*. 2003;**170**:135-141.
Crossref | CAS | Web of Science® | Google Scholar

28 Lihong B, Wurentuya WW, Tegus O. A new route for the synthesis of submicron-sized LaB_6. *Mater Charact*. 2014;**97**:69-73.
Crossref | Web of Science® | Google Scholar

29 Pan WY, Bao QW, Mao YJ, et al. Low-temperature synthesis of nanosized metal borides through reaction of lithium borohydride with metal hydroxides or oxides. *J Alloy Compd*. 2015;**651**:666-672.
Crossref | CAS | Web of Science® | Google Scholar

30 de Resende WG, De Grave E, da Costa GM, et al. Influence of the borohydride concentration on the composition of the amorphous Fe-B alloy produced by chemical reduction of synthetic, nano-sized iron-oxide particles. Part I: Hematite. *J Alloy Compd*. 2007;**440**:236-247.
Crossref | Web of Science® | Google Scholar

31 Mao W, Bao K, Liu G, et al. Synthesis of orthorhombic chromium boride by solid state reaction. *J Superhard Mater*. 2016;**38**:251-254.

solid-state reaction. *Scripta Mater*. 2015;**109**:100-103.

33 Toby BH, Von Dreele RB. {\it GSAS-II} : the genesis of a modern open-source all purpose crystallography software package. *J Appl Crystallogr*. 2013;**46**:544-549.
Wiley Online Library | CAS | Web of Science® | Google Scholar

34 Scherrer P. Determination of the size and internal structure of colloidal particles using X-rays. *Math-Phys Kl*. 1918;**40**:98-100.
Google Scholar

35 Momma K, Izumi F. {\it VESTA3} for three-dimensional visualization of crystal, volumetric and morphology data. *J Appl Crystallogr*. 2011;**44**:1272-1276.
Wiley Online Library | CAS | Web of Science® | Google Scholar

36 Mitchell DRG. DiffTools: electron diffraction software tools for DigitalMicrographTM. *Microsc Res Techniq*. 2008;**71**:588-593.
Wiley Online Library | CAS | PubMed | Web of Science® | Google Scholar

37 Zhao T, Rønning M, Chen D. Preparation of nanocrystalline Na_2ZrO_3 for high-temperature CO_2 acceptors: chemistry and mechanism. *J Energy Chem*. 2013;**22**:387-393.
Crossref | CAS | Web of Science® | Google Scholar

38 Cable M, Fernandes MHV. Volatilisation of molten sodium metaborate with convection of the furnace atmosphere. *Phys Chem Glasses*. 1998;**39**:228-235.
http://www.ingentaconnect.com/content/sgt/pcg/1998/00000039/00000004/3904228 .
CAS | Web of Science® | Google Scholar

39 Shi L, Gu Y, Chen L, et al. A convenient solid-state reaction route to nanocrystalline TiB_2. *Inorg Chem Commun*. 2004;**7**:192-194.
Crossref | CAS | Web of Science® | Google Scholar

40 Zhang X, Hilmas GE, Fahrenholtz WG. Synthesis, densification, and mechanical properties of TaB_2. *Mater Lett*. 2008;**62**:4251-4253.
Crossref | CAS | Web of Science® | Google Scholar

Soc. 2010;**93**:1586-1590.
Wiley Online Library | CAS | Web of Science® | Google Scholar